

**Epitaxial growth of black phosphorene enabled on black-phosphorene-like group IV-VI substrates**M. U. Muzaffar <sup>1</sup>, Xue-Sen Wang <sup>2,3</sup>, Shunhong Zhang <sup>1</sup>, Ping Cui <sup>1,\*</sup> and Zhenyu Zhang <sup>1,†</sup><sup>1</sup>*International Center for Quantum Design of Functional Materials (ICQD), Hefei National Laboratory for Physical Sciences at Microscale (HFNL), and CAS Center for Excellence in Quantum Information and Quantum Physics, University of Science and Technology of China, Hefei, Anhui 230026, China*<sup>2</sup>*Department of Physics, National University of Singapore, 2 Science Drive 3, Singapore, 117542, Singapore*<sup>3</sup>*Center for Topological Functional Materials, and Henan Key Laboratory of Photovoltaic Materials, Henan University, Kaifeng, Henan 475004, China*

(Received 21 December 2020; revised 31 October 2021; accepted 4 November 2021; published 13 December 2021)

Black phosphorene (BlackP) is a promising two-dimensional material for next-generation nanoelectronics with a thickness-dependent bandgap and high carrier mobility. Yet to date, epitaxial growth of BlackP on a proper substrate remains a daunting challenge, which in turn prevents its mass production for device applications. Here we propose that BlackP-like group IV-VI substrates can be ideal candidates to promote epitaxial growth of BlackP. We first show, using first-principles approaches, that BlackP is energetically and thermodynamically stable on SnSe(001) as a representative substrate, which can be attributed to the isovalency nature and inherent structural similarity between the two. In contrast, as a close isomer of BlackP, blue phosphorene is thermodynamically unstable on SnSe(001). Next, we show that two phosphorus adatoms not only can readily form a dimer via P-P attraction, but such dimers also can diffuse isotropically and much faster than P monomers, both aspects highly desirable for initial growth and mass production of BlackP. Furthermore, BlackP grown on such semiconducting substrates can be directly exploited as a platform for novel optoelectronic devices, as demonstrated using the BlackP/SnSe heterobilayer that possesses a type-II band alignment and favors the formation of indirect excitons with desirable functionalities.

DOI: [10.1103/PhysRevB.104.235415](https://doi.org/10.1103/PhysRevB.104.235415)**I. INTRODUCTION**

Since the mechanical exfoliation of graphene from graphite [1], much research effort has been devoted to two-dimensional (2D) materials, exploring their exotic properties and potential technological applications [2–4]. Beyond graphene, the discoveries of other 2D systems, such as silicene [5], phosphorene [6,7], borophene [8,9], stanene [10], bismuthene [11], tellurene [12], hexagonal boron nitride (*h*-BN) [13], and transition metal dichalcogenides (TMDs) [14,15], have greatly expanded the 2D materials family. Each family member invokes different synthesis methods pertaining to its unique chemical properties and morphological structures. As we go from initial materials discoveries to potential device applications, the success of each of the enchanted 2D materials depends on the development of efficient and scalable methods for fabricating large-area and high-quality crystalline samples. In this regard, epitaxial growth on proper substrates has been widely explored, as representatively demonstrated for graphene [16–19], *h*-BN [20,21], and other 2D systems [22–25].

Among the rising stars of the 2D materials family, black phosphorene (BlackP) has attracted much limelight since its exfoliation from its bulk form, owing to its thickness-dependent bandgap and high carrier mobility [26,27]. In

addition to BlackP, blue phosphorene (BlueP) has also been predicted to be an energetically comparable isomer with unique properties of its own [28], and several substrates have been explored to promote its epitaxial growth [29–31], including the prediction and experimental observation of an intriguing half-layer-by-half-layer growth mode [30,31]. To date, extensive efforts have been made on epitaxial growth of BlackP both theoretically [32,33] and experimentally [34–36] as well, but with only limited success. Of particular note was the recent experimental demonstration of epitaxial growth of BlackP on an elegantly functionalized Si/SiO<sub>2</sub> substrate invoking complex precursors and surface chemical reactions [36] and growth of few-layer BlackP on mica promoted by BlackP fragments from a bulk black phosphorus source [37]. To fully exploit the application potentials of BlackP, major advances are still critically needed, ideally involving much simpler precursors and more straightforward kinetic pathways. Such advances are likely to be enabled by the identification of more fertile substrates with optimal interfacial couplings.

In this paper, we propose a straightforward yet conceptually intuitive approach to fabricating BlackP via epitaxial growth, as promoted by BlackP-like group IV-VI substrates that possess both structural and chemical affinities [38,39]. We first show, using first-principles approaches, that BlackP is energetically and thermodynamically stable on SnSe(001) as a representative substrate. In contrast, BlueP is thermodynamically unstable on SnSe(001), due to distinct structural dissimilarity. The vital role of structural similarity as revealed

\*Corresponding authors: cuipeg@ustc.edu.cn

†Corresponding authors: zhangzy@ustc.edu.cn

here is transformative, and is broadly applicable in van der Waals (vdW) epitaxy that possesses strong lateral bonding but weak vertical/interlayer coupling. Next, we study the corresponding atomistic growth mechanisms and reveal that two phosphorus adatoms not only can readily form a dimer on SnSe(001) via effective P-P attraction, but such dimers also can diffuse isotropically and much faster than the P monomer counterparts, both aspects highly desirable for initial growth and eventual mass production of BlackP [40,41]. Furthermore, a BlackP overlayer grown on such semiconducting substrates can be directly exploited as a platform for novel optoelectronic devices, as demonstrated using the BlackP/SnSe heterobilayer, which possesses a type-II band alignment and favors the formation of indirect excitons with desirable properties.

The paper is organized as follows. In Sec. II, we briefly describe the model systems and details of the computational methods. In Sec. III, we first introduce the design principle and selection of proper substrates, and then show that the BlackP-like SnSe can be an ideal candidate substrate to promote the epitaxial growth of BlackP based on the first-principles calculations surrounding the energetics, thermodynamic stabilities, and atomistic growth mechanisms at the initial stages. Afterwards, we reveal a type-II band alignment of the resulting BlackP/SnSe heterostructures, with novel catalytic and optoelectronic properties. In the last part of this section, we briefly discuss the physically realistic growth aspects of the present study. Finally, we conclude in Sec. IV.

## II. COMPUTATIONAL METHODS

The density functional theory (DFT) calculations were performed using the projector-augmented wave method [42] implemented in the Vienna *ab initio* simulation package (VASP) [43], with the Perdew-Burke-Ernzerhof (PBE) exchange and correlation functional [44]. The kinetic energy cutoff of the plane-wave basis was chosen to be 400 eV, and the Brillouin zone (BZ) was sampled by Monkhorst-Pack  $k$  mesh with a density of  $2\pi \times 0.02/\text{\AA}$ . To account for the vdW interactions between P adatoms/layer and the group IV-VI substrates, the semiempirical dispersion-corrected DFT-D3 method [45] by Grimme was employed. The convergences of force for geometry optimization and total energy for electron wave function self-consistency were set to be 0.02 eV/\AA and  $10^{-5}$  eV, respectively. To obtain more reliable electronic bandgaps, the HSE06 hybrid functional [46] was used.

To mimic a semi-infinite solid, a four-layer slab model for the group IV-VI substrates was used with the bottom layer fixed at their bulk positions during the structural optimization, and a vacuum of more than 15 \AA was added along the direction perpendicular to the surface. The lattice constants of bulk SnSe were obtained by fully relaxing with variable unit cell volumes. The  $a$  and  $b$  lattices (surface lattices) of the constructed supercells for BlackP/SnSe, BlueP/SnSe, and all the adsorption systems adopt the values of the SnSe bulk because the lattice of the substrate cannot be noticeably changed by the overlayer or adatoms during a realistic growth process. In addition, we have examined a  $(4 \times 4)$  SnSe(001) surface and did not observe a surface reconstruction during relaxation. To make the demanding computation affordable, the SnSe(001)

TABLE I. Optimized structural properties of the BlackP and group IV-VI binary compounds, including in-plane lattice constants ( $a$ ,  $b$ ), lattice anisotropy ( $b/a$ ), and lattice mismatches defined by  $\delta_1 = |a_{\text{sheet}} - a_{\text{sub}}|/a_{\text{sub}}$  and  $\delta_2 = |b_{\text{sheet}} - b_{\text{sub}}|/b_{\text{sub}}$ , where  $a_{\text{sheet}}$ ,  $b_{\text{sheet}}$ ,  $a_{\text{sub}}$ , and  $b_{\text{sub}}$  are the supercell parameters of the BlackP and group IV-VI substrates, respectively.

System	$a(\text{\AA})$	$b(\text{\AA})$	$b/a$	$\delta_1$ (%)	$\delta_2$ (%)
BlackP	3.30	4.59	1.39	–	–
GeS	3.66	4.44	1.21	9.83	3.37
GeSe	3.86	4.52	1.17	14.50	1.54
SnS	3.99	4.41	1.10	3.38	4.08
SnSe	4.17	4.53	1.08	1.07	1.32

surface was modeled using a  $(3 \times 3)$  surface supercell to investigate the diffusion behaviors of P adatoms, with the aid of the climbing-image Nudged Elastic Band (cNEB) method [47], and the structural convergence criterion was similar to those used in the above-mentioned structural optimization.

The *ab initio* molecular dynamics (AIMD) simulations were performed to verify the thermodynamic stability. The canonical NVT (N, number of particles; V, volume; T, temperature) ensemble was adopted by using the algorithm of Nosé thermostat [48], with the time step of 2 fs. During the AIMD simulations, the bottom two layers of the SnSe(001) surface were fixed at their bulk positions.

## III. RESULTS AND DISCUSSIONS

### A. Design principle and selection of proper substrates for epitaxial growth of BlackP

The central design principle in our searching for fertile substrates to promote epitaxial growth of BlackP is the structural similarity and equivalence in valence electrons (isovalency). The enabling power of the former is elegantly encoded in the nature of vdW epitaxy, where the intralayer coupling is strong, while the interfacial binding is rather weak, allowing the structural similarity between the growing layer and substrate to play a more decisive role in selecting the preferred growth mode. Empowered with this design principle, we choose group IV-VI binary compounds (i.e., GeS, GeSe, SnS, and SnSe) as candidate substrates, possessing equivalent valence electrons per formula unit (namely, “4+6=5+5”) and usually adopting an orthorhombic layered structure similar to black phosphorus [38,39]. In spite of the elemental difference, both the BlackP overlayer and IV-VI substrates possess distinct ridges along one of the crystalline directions [Figs. 1(a) and 1(b)], again a favorable aspect when epitaxial growth is concerned. Generally, their ridge structures exhibit a larger lattice parameter along the armchair direction ( $b$  axis) than that along the zigzag direction ( $a$  axis). As shown in Table I, the lattice constants of the group IV-VI substrates along the  $b$  axis are reasonably comparable to the value of BlackP, while those along the  $a$  axis exhibit significant increments from GeS to SnSe. These results indicate that, even on GeS, a  $(1 \times 1)$  overlayer of BlackP would still experience a very large lattice mismatch ( $\delta$ ) of  $\sim 10\%$  in one direction, which is energetically too costly [49]. On the other hand, the lattice anisotropy

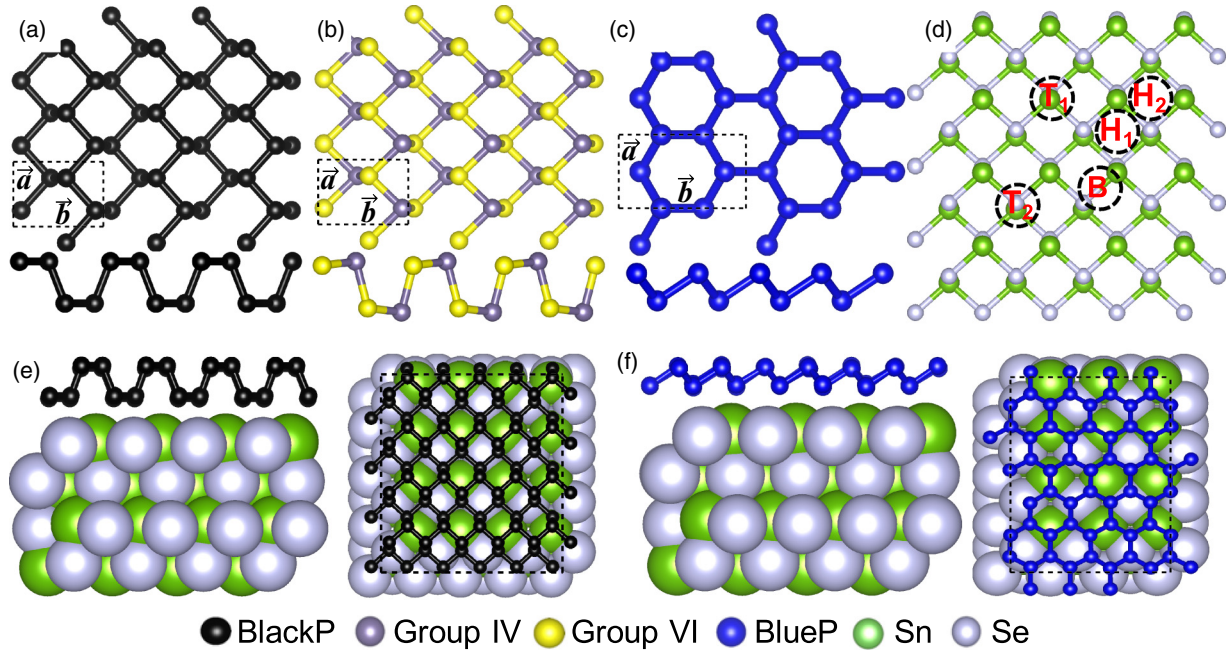


FIG. 1. Top (upper panel) and side (lower panel) views of the atomic structures of (a) BlackP, (b) group IV-VI monolayer, and (c) BlueP, with the corresponding unit cells indicated by the dashed rectangles. (d) Five high-symmetry adsorption sites on SnSe(001). Side (left panel) and top (right panel) views of the most stable configurations of (e) BlackP and (f) BlueP on SnSe(001), with the minimal matching supercells indicated by the dashed rectangles.

( $b/a$ ) follows BlackP > GeS > GeSe > SnS > SnSe. This observation, plus the fact that the interlayer coupling between the BlackP overlayer and substrate is expected to be rather weak [32], inspires us to consider superstructures that can minimize  $\delta$  along both directions, as detailed next.

In searching for minimized  $\delta$ , we have considered ( $1 \times 1$ ) overlayers of BlackP on GeS(001) and GeSe(001), as well as ( $5 \times 4$ ) superstructures of BlackP on ( $4 \times 4$ ) surfaces of SnS(001) and SnSe(001), with the results shown in Table I. Among the candidate systems, BlackP/SnSe(001) exhibits the lowest  $\delta$  of 1.07% and 1.32% along the zigzag and armchair directions, respectively. In comparison, for BlueP with the lattice constants of  $a = 3.27 \text{ \AA}$  and  $b = 5.67 \text{ \AA}$  [Fig. 1(c)] [50], BlueP/SnSe(001) also has the lowest  $\delta$  of 4.55% and 6.12% along the zigzag and armchair directions, respectively, given by the matching relationship of ( $4 \times 3$ ) BlueP and ( $3 \times 4$ ) SnSe(001). Based on these considerations, in the remaining paper we concentrate on SnSe(001) with the lowest mismatches for both isomers as the representative substrate to promote epitaxial growth.

### B. Energetics and stability of BlackP/BlueP on SnSe(001)

To find the energetically stable structures of BlackP and BlueP on SnSe(001), different initial configurations are considered, containing one P atom placed at one of the high-symmetry sites, defined on top of an Sn atom ( $T_1$  site), an Se atom ( $T_2$  site), a bridge site between Sn and Se (B site), and two hollow sites of Sn-Se rings ( $H_1$  site and  $H_2$  site) [Fig. 1(d)]. After structural optimization, the configuration associated with the  $H_1$  site stays as the most stable structure, as shown in Figs. 1(e) and 1(f), with the  $T_1$ ,  $T_2$ , and B configurations converting into this structure. The configuration

associated with the  $H_2$  site is a metastable one. To quantify the stability of both monolayers on SnSe(001), we have calculated the binding energies per P atom, defined by  $E_b = (E_{\text{sub}} + N \times E_1 - E_t)/N$ . Here  $E_{\text{sub}}$ ,  $E_1$ , and  $E_t$  represent the total energies of the substrate, one P atom in freestanding BlackP or BlueP, and the combined system, respectively, and  $N$  is the total number of P atoms within the supercell. The calculated binding energies are 0.10 and 0.06 eV per P atom for BlackP/SnSe(001) and BlueP/SnSe(001), respectively, displaying the same relative stability trend as in the freestanding form. Here it is also worthwhile to emphasize that, even though both BlackP and BlueP are energetically stable at zero temperature, the interfacial binding energies are in the weak regime using the criterion of an earlier study [32]. The difference in the interfacial interactions of the two systems can be manifested by different thermodynamic stabilities, as shown next.

In realistic experiments, such monolayers must be synthesized at finite temperatures, where thermal perturbations are bound to induce structural defects and potentially compromise the geometrical integrity of the overlayers. To examine the thermal stability of BlackP and BlueP on SnSe(001), we have performed AIMD simulations at 300 K, well below the thermal degradation temperature ( $\sim 400^\circ\text{C}$ ) for few-layer BlackP [32,51]. In these simulations, we doubled the supercell sizes shown in Figs. 1(e) and 1(f) along both the  $b$  and  $a$  axes to allow the systems to reconstruct freely at the given temperature. The results are contrasted in Fig. 2, showing that, after 5 ps, the BlackP monolayer retains the structure intact, while BlueP fails to maintain the ordered structure against thermal perturbations. Accordingly, the total energy fluctuation for BlackP is stabilized beyond a transient period [Fig. 2(c)], confirming its high thermal stability; in contrast, the total energy

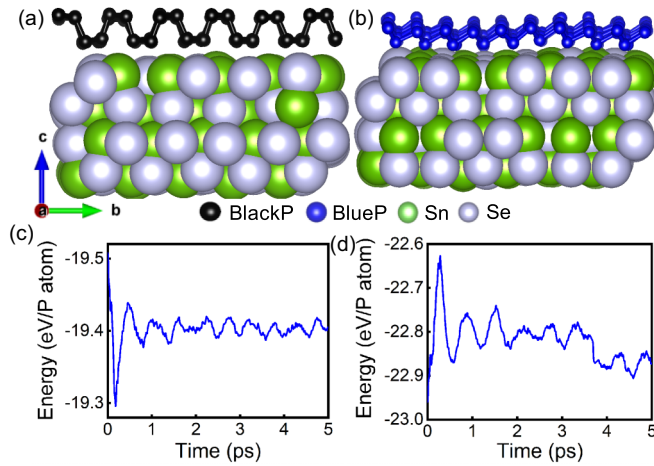


FIG. 2. Contrasting thermodynamic stabilities of (a) BlackP and (b) BlueP on SnSe (001) after 5-ps AIMD simulations at 300 K. The corresponding energy evolutions are contrasted in (c) and (d).

for BlueP is decreasing significantly, signifying its thermal instability. Based on these analyses, we confirm that BlackP monolayer with energetic and thermodynamic stabilities is highly probable to be readily synthesized on the BlackP-like SnSe(001) substrate, while BlueP on this substrate would be unstable at least at room temperature. Furthermore, given the close energetic stabilities of BlackP and BlueP, their structural transition can be induced under ambient conditions by other physical knobs such as the pressure, as demonstrated in few-layer BlackP and BlueP [52] or in the corresponding bulk phases [53].

### C. Atomistic mechanism in the initial growth stages of BlackP on SnSe(001)

To reveal potential nucleation behaviors of P atoms on SnSe(001), we investigate the adsorption of P monomers, dimerization of two P monomers, as well as their mobilities [40]. For the adsorption of one P atom, similar to the monolayer case, the  $H_1$ -site adsorption configuration is found to be most stable and the  $H_2$ -site configuration is metastable. The corresponding adsorption energy  $E_{\text{ads}}$  on the  $H_1$  site is  $-3.64$  eV, calculated by  $E_{\text{ads}} = E_{\text{Pmono+sub}} - E_{\text{Pmono}} - E_{\text{sub}}$ , where  $E_{\text{Pmono+sub}}$ ,  $E_{\text{Pmono}}$ , and  $E_{\text{sub}}$  are the total energies of the whole system, an isolated P atom in gas phase, and the SnSe(001) substrate respectively. When two P atoms are placed on the surface, they prefer to form a dimer with a P-P distance of  $1.94$  Å rather than stay apart (see Fig. S1 in the Supplemental Material [54]). The dimer adsorption energy is defined as  $E_{\text{ads}} = E_{\text{Pdim+sub}} - E_{\text{Pdim}} - E_{\text{sub}}$ , where  $E_{\text{Pdim+sub}}$  and  $E_{\text{Pdim}}$  are the total energies of the combined system and an isolated P dimer in the gas phase, respectively. The resulting  $E_{\text{ads}}$  is  $-0.62$  eV, ensuring the stability of a P dimer on the substrate. It is noted that, even though the energy gain upon adsorption is only  $0.62$  eV, the P dimers should stay on the substrate during supersaturation of dimers in the gas phase. As expected, the formation of a P dimer is attributable to the isovalency nature of the overlayer and substrate. The P-P attraction on SnSe(001) as revealed here is distinctly different from the repulsive interactions on sev-

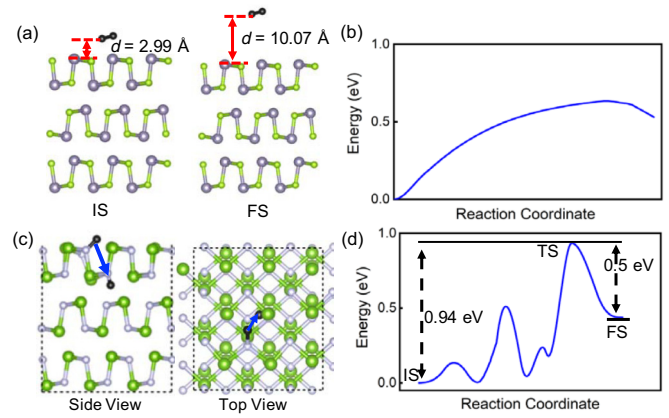


FIG. 3. (a) Side views of the initial state (IS, left panel) and final state (FS, right panel) for a P dimer desorption process on SnSe(001). The minimal distance  $d$  between the dimer and substrate is  $2.99$  and  $10.07$  Å, respectively. (b) Energy Profile of the desorption process. (c) Schematic representation of the diffusion pathway of a P adatom from the surface to subsurface on SnSe(001), and the corresponding energy profile is given in (d). TS represents the transition state.

eral other substrates studied previously, including Cu(111), Au(111), and GaN(001) [30,55]. Such an attractive behavior of the P adatoms is clearly advantageous to the islanding and subsequent growth of phosphorene overlayers. Furthermore, we have calculated the desorption energy barrier of a P dimer from the substrate to the gas phase to be  $0.65$  eV [see Figs. 3(a) and 3(b)]. Here, the most stable adsorption configuration is taken as the initial state, and an optimized adsorption configuration with the minimal distance  $d$  between the P dimer and substrate being  $10.07$  Å serves as the final state in carrying out the cNEB calculations. In addition, we have estimated the dissociation energy of a P dimer on the substrate to be  $-2.01$  eV, which is defined as  $E_{\text{disso}} = E_{\text{Pdim+sub}} - 2 \times E_{\text{Pmono+sub}} + E_{\text{sub}}$ . Such a large dissociation energy further confirms the stability of the P ad-dimers.

Beyond adsorption, the mobility of monomers and dimers is another vital kinetic aspect in epitaxial growth, especially with regard to fabricating large-area and homogeneous samples. To this end, we explore different possible diffusion pathways for migration of both P monomers and dimers on SnSe(001). For a P monomer moving between two neighboring  $H_1$  sites, the structural asymmetry of the substrate results in two distinct diffusion pathways, one along the armchair direction ( $H_1 \rightarrow A_1$ ), and the other along the zigzag direction ( $H_1 \rightarrow Z_1$ ), as shown in Fig. 4(a), with the corresponding diffusion barriers of  $0.61$  and  $0.91$  eV [Fig. 4(b)]. We have also calculated the diffusion barrier of a P monomer between the neighboring  $H_1$  and  $H_2$  sites, showing a much larger value than the above two. For P-P dimers as shown in Figs. 4(c) and 4(d), the diffusion barriers are significantly reduced to  $0.43$  and  $0.41$  eV along the zigzag and armchair directions, respectively, yielding a high reaction rate of  $1.91 \times 10^6$  s $^{-1}$  at 300 K. The reaction rate is estimated by the Arrhenius equation of  $A \exp[-E_a/(K_B T)]$ , where  $E_a$  is the diffusion barrier,  $K_B$  the Boltzmann constant,  $T$  the temperature, and the prefactor  $A$  is  $\sim 10^{13}$  s $^{-1}$ . Crucially, the dimer diffusion barriers are substantially lower than the dimer

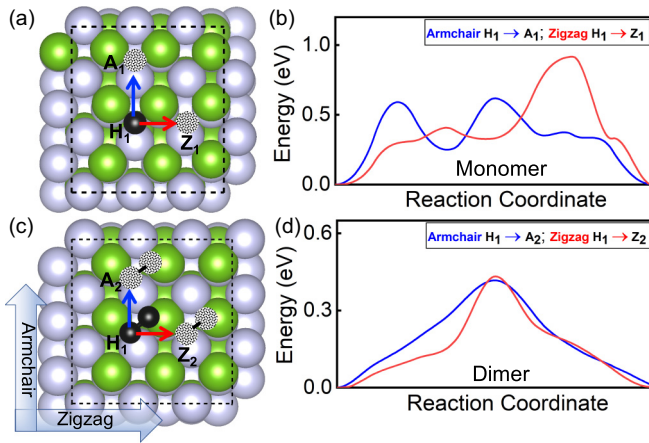


FIG. 4. (a) Diffusion pathways of a P monomer on SnSe(001), and the corresponding energy profiles along the armchair and zigzag directions are presented in (b). (c) and (d) Same as (a) and (b), but for the case of an adsorbed P-P dimer. The solid and dotted black balls represent the initial and final positions of the P adatom or dimer, respectively.

desorption barrier (0.65 eV), ensuring sufficient mobilities of the P dimers on the substrate at proper growth temperatures at which the dimers do not desorb effectively from the substrate at the supersaturation conditions. A more subtle aspect is that the diffusions of P-P dimers are essentially isotropic over the entire surface, which is hugely beneficial for fabricating large-area and homogeneous samples [40]. The underlying reason of a stable and fast diffusing dimer on SnSe(001) is inherently rooted in the relative binding strengths of P-P and P-substrates [56]. Here we note that such dimer feeding behaviors have also been proposed in the initial growth stages of graphene on Cu substrates [41], resulting in the growth of large-area and high-quality samples as observed [16,57]. From a fundamental aspect, future definitive experimental validations of such dimer dominant growth modes in either graphene or phosphorene epitaxy on proper substrates would further enrich our understanding of atomistic mechanisms in nonequilibrium growth [40,58].

To examine the tendency of the P adatoms diving into the subsurface, we further investigate the adsorption energetics and selective diffusion barriers of a P monomer and a P-P dimer in the subsurface of SnSe. We find that both the P monomer and dimer on the subsurface are less stable than that on the surface, by 0.44 and 0.71 eV/P atom, respectively. The diffusion barrier of a P adatom from the surface to subsurface is 0.94 eV [Figs. 3(c) and 3(d)]. Though this barrier is comparable to that on the surface, the reverse process of a P atom returning from the subsurface to surface has a much lower barrier of 0.50 eV, leading to the high preference of the P atoms to the surface. Based on these calculations, we conclude that the P atoms highly prefer to stay on the surface rather than diving into the subsurface. Overall, we infer that the P adatoms can readily form P-P dimers, and once formed such dimers can even much more rapidly diffuse and join growing phosphorene islands on SnSe(001), leading to the formation of larger islands that prefer to adopt the energetically favorable and thermodynamically stable BlackP.

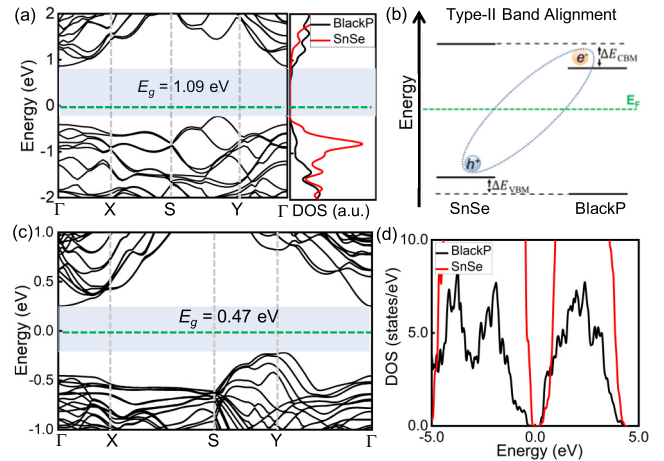


FIG. 5. (a) Band structure and density of states (DOS) of a BlackP/SnSe heterobilayer, calculated using the HSE06 method. (b) Schematic representation of the corresponding type-II band alignment. Here, an electron and a hole within an indirect exciton are separated by a built-in interlayer field. (c) Band structure and (d) DOS of a BlackP monolayer on a SnSe(001) surface modeled by a four-layer slab with the bottom layer fixed at its bulk position, obtained within the PBE scheme.

#### D. Type-II band alignment and indirect excitons in BlackP on SnSe(001)

The anticipated success in the synthesis of BlackP on the semiconducting SnSe substrate will not only overcome the standing challenge of its epitaxial growth, but also offer a physically realistic material platform to explore its emergent properties and potential applications, even without the need to transfer. Here, by taking the BlackP/SnSe heterobilayer as an example, we highlight two aspects to illustrate the expected significance of such heterostructures in the fast-growing field of 2D materials physics, namely, the type-II electronic band alignment, and the indirect excitons. We first calculate the electronic structures of BlackP and SnSe monolayers, as presented in Fig. S2 in the Supplemental Material [54]. The band structures indicate that the BlackP monolayer possesses a direct bandgap of 1.52 eV at the  $\Gamma$  point, while the SnSe monolayer exhibits an indirect bandgap of 1.61 eV. The BlackP/SnSe heterobilayer is further calculated to exhibit an indirect band gap of 1.09 eV, with the valence band maximum (VBM) dominated by the SnSe layer and conduction band minimum (CBM) mainly contributed by the BlackP layer, as shown in [Fig. 5(a)]. Such features characterize the BlackP and SnSe monolayers to form a type-II band alignment through the vdW interactions [59,60]. Indeed, our calculations reveal that the CBM and VBM of the BlackP monolayer are, respectively, lower in energy than that of the SnSe monolayer, with the valence and conduction band offsets of the heterobilayer being  $\Delta E_{\text{VBM}} = 0.21$  eV and  $\Delta E_{\text{CBM}} = 0.29$  eV [Fig. 5(b)]. These band edges are the relevant states upon optical excitation, and the lowest-energy electron-hole pairs are thus spatially separated in the BlackP and SnSe layers, forming indirect excitons [60–65]. Our detailed calculations also show that such a distinct feature is preserved even when the SnSe layer is further increased to

the multilayer regime [Figs. 5(c) and 5(d)]. Here we note that quantitatively reliable determinations of the binding energies of such excitons defined in the heterostructures are technically demanding, especially within the state-of-the-art *GW*-Bethe-Salpeter equation (*GW*-BSE) approach [66–69], but their very existence and indirect nature are unquestionable.

Given the spatially separated or indirect nature of the excitons in such heterostructures, various superior functionalities can be envisioned, as such excitons will have longer lifetime and higher mobility. One is from the individual exciton level, namely, the heterostructures may have desirable photocatalytic performance in energy conversion processes such as photolysis [70]. The other is from the collective level, namely, such indirect excitons beyond the widely studied TMD heterostructures can serve as new and advantageous materials for realizing exciton condensation [71,72]. In particular, when compared with the TMD heterostructures, the present heterobilayer consists of elemental BlackP monolayer as one constituent layer, which has higher carrier mobility. Furthermore, SnSe is a well-known ferroelectric 2D material [73,74], offering an extra degree of freedom in the tunability.

### E. Growth perspective/prospectives

Here, we briefly discuss the physically realistic growth aspects of the present study. First, the enabling power of isovalency and isostructure as a new design principle as introduced here was already partially supported by the recent experimental growth of BlackP-like antimonene on the SnSe substrate by molecular beam epitaxy [75]. Even though the importance of the isostructural aspect was not explicitly recognized or emphasized, the preference of the antimonene in the BlackP-like phase ( $\alpha$ -antimonene) to the BlueP-like phase ( $\beta$ -antimonene) can now be attributed to the promotion of the BlackP-like SnSe substrate. In contrast, many other substrates have been shown to prefer the growth of  $\beta$ -antimonene [76–80]. Stimulated by the central idea of this work, an experimental effort has further demonstrated the enabling power of structural similarity in vdW epitaxy by successfully growing various binary group-V alloys in the BlackP-like phase with tunable electronic properties [81]. Secondly, besides the proper choice of a substrate, another crucial factor in growth of BlackP is the source of phosphorus. A typical phosphorus source will supply vaporous  $P_4$  molecules at relatively low temperatures, and such  $P_4$  molecules start to dissociate to  $P_2$  above 800°C

[29], which is comparable to the melting temperature of the SnSe substrate (at 861°C). To avoid damaging the substrate, proper phosphorus sources such as InP [31] can be used, or alternatively a valve phosphorus cracker can be applied to generate  $P_2$  molecules, which are also predicted here to be the main feeding species during the growth of BlackP on SnSe. We expect such efforts will not only lead to realization of the epitaxial growth of BlackP, but will also offer unprecedented insights into the underlying atomistic growth kinetics involved [40,58].

## IV. CONCLUSIONS

In conclusion, following the intuitive structural similarity consideration and isovalency rule, we have identified a BlackP-like IV-VI substrate, namely, SnSe(001), as an ideal candidate to promote epitaxial growth of BlackP. Our comparative studies have shown that BlackP is energetically and thermodynamically stable on SnSe(001); in contrast, the energetically degenerate isomer of BlueP on SnSe(001) would be unstable against thermodynamic disturbance. Furthermore, we have revealed that two phosphorus adatoms not only can readily form a dimer on SnSe(001), but such dimers also can diffuse isotropically and much faster than the P monomer counterparts, both aspects highly desirable for further growth and eventual mass production of BlackP. Moreover, the resulting heterostructures have been shown to exhibit a type-II band alignment, offering physically realistic platforms for realization of indirect excitons that in turn can be exploited for various emergent properties and superior functionalities.

## ACKNOWLEDGMENTS

This work was supported by the National Key R&D Program of China (Grant No. 2017YFA0303500), the National Natural Science Foundation of China (Grants No. 11634011, No. 11974323, No. 11722435, and No. 11904350), the Strategic Priority Research Program of Chinese Academy of Sciences (Grant No. XDB30000000), and the Anhui Initiative in Quantum Information Technologies (Grant No. AHY170000). S.Z. acknowledges the support of the initiative program of USTC and Anhui Provincial Natural Science Foundation (Grant No. 2008085QA30). M.U.M would like to thank the support from the Distinguished/Outstanding Postdoctoral Fellowships of the Hefei National Laboratory for Physical Sciences at the Microscale.

- 
- [1] K. S. Novoselov, A. K. Geim, S. V. Morozov, D. Jiang, Y. Zhang, S. V. Dubonos, I. V. Grigorieva, and A. A. Firsov, *Science* **306**, 666 (2004).
  - [2] K. S. Novoselov, V. I. Fal'ko, L. Colombo, P. Gellert, M. Schwab, and K. Kim, *Nature (London)* **490**, 192 (2012).
  - [3] K. S. Novoselov, A. Mishchenko, A. Carvalho, and A. H. Castro Neto, *Science* **353**, aac9439 (2016).
  - [4] D. Akinwande, C. Huyghebaert, C.-H. Wang, M. I. Serna, S. Goossens, L.-J. Li, H.-S. P. Wong, and F. H. L. Koppens, *Nature (London)* **573**, 507 (2019).
  - [5] P. Vogt, P. De Padova, C. Quaresima, J. Avila, E. Frantzeskakis, M. C. Asensio, A. Resta, B. Ealet, and G. Le Lay, *Phys. Rev. Lett.* **108**, 155501 (2012).
  - [6] L. Li, Y. Yu, G. J. Ye, Q. Ge, X. Ou, H. Wu, D. L. Feng, X. H. Chen, and Y. Zhang, *Nat. Nanotechnol.* **9**, 372 (2014).
  - [7] H. Liu, A. T. Neal, Z. Zhu, Z. Luo, X. Xu, D. Tománek, and P. D. Ye, *ACS Nano* **8**, 4033 (2014).
  - [8] A. J. Mannix, X.-F. Zhou, B. Kiraly, J. D. Wood, D. Alducin, B. D. Myers, X. Liu, B. L. Fisher, U. Santiago, J. R. Guest, M. J. Yacaman, A. Ponce, A. R. Oganov, M. C. Hersam, and N. P. Guisinger, *Science* **350**, 1513 (2015).

- [9] B. Feng, J. Zhang, Q. Zhong, W. Li, S. Li, H. Li, P. Cheng, S. Meng, L. Chen, and K. Wu, *Nat. Chem.* **8**, 563 (2016).
- [10] F.-F. Zhu, W.-J. Chen, Y. Xu, C.-L. Gao, D.-D. Guan, C.-H. Liu, D. Qian, S.-C. Zhang, and J.-F. Jia, *Nat. Mater.* **14**, 1020 (2015).
- [11] F. Reis, G. Li, L. Dudy, M. Bauernfeind, S. Glass, W. Hanke, R. Thomale, J. Schäfer, and R. Claessen, *Science* **357**, 287 (2017).
- [12] Z. Zhu, X. Cai, S. Yi, J. Chen, Y. Dai, C. Niu, Z. Guo, M. Xie, F. Liu, J.-H. Cho, Y. Jia, and Z. Y. Zhang, *Phys. Rev. Lett.* **119**, 106101 (2017).
- [13] L. Song, L. Ci, H. Lu, P. B. Sorokin, C. Jin, J. Ni, A. G. Kvashnin, D. G. Kvashnin, J. Lou, B. I. Yakobson, and P. M. Ajayan, *Nano Lett.* **10**, 3209 (2010).
- [14] B. Radisavljevic, A. Radenovic, J. Brivio, V. Giacometti, and A. Kis, *Nat. Nanotechnol.* **6**, 147 (2011).
- [15] Q. H. Wang, K. Kalantar-Zadeh, A. Kis, J. N. Coleman, and M. S. Strano, *Nat. Nanotechnol.* **7**, 699 (2012).
- [16] X. Li, W. Cai, J. An, S. Kim, J. Nah, D. Yang, R. Piner, A. Velamakanni, I. Jung, E. Tutuc, S. K. Banerjee, L. Colombo, and R. S. Ruoff, *Science* **324**, 1312 (2009).
- [17] K. S. Kim, Y. Zhao, H. Jang, S. Y. Lee, J. M. Kim, K. S. Kim, J.-H. Ahn, P. Kim, J.-Y. Choi, and B. H. Hong, *Nature (London)* **457**, 706 (2009).
- [18] Y. F. Hao, M. S. Bharathi, L. Wang, Y. Y. Liu, H. Chen, S. Nie, X. H. Wang, H. Chou, C. Tan, B. Fallahzad, H. Ramanarayan, C. W. Magnuson, E. Tutuc, B. I. Yakobson, K. F. McCarty, Y.-W. Zhang, P. Kim, J. Hone, L. Colombo, and R. S. Ruoff, *Science* **342**, 720 (2013).
- [19] M. Wang, M. Huang, D. Luo, Y. Li, M. Choe, W. K. Seong, M. Kim, S. Jin, M. Wang, and S. Chatterjee, *Nature (London)* **596**, 519 (2021).
- [20] L. Wang, X. Xu, L. Zhang, R. Qiao, M. Wu, Z. Wang, S. Zhang, J. Liang, Z. H. Zhang, Z. B. Zhang, W. Chen, X. Xie, J. Zong, Y. Shan, Y. Guo, M. Willinger, H. Wu, Q. Li, W. Wang, P. Gao, S. Wu, Y. Zhang, Y. Jiang, D. Yu, E. Wang, X. Bai, Z.-J. Wang, F. Ding, and K. Liu, *Nature (London)* **570**, 91 (2019).
- [21] T.-A. Chen, C.-P. Chuu, C.-C. Tseng, C.-K. Wen, H.-S. P. Wong, S. Y. Pan, R. T. Li, T.-A. Chao, W.-C. Chueh, Y. F. Zhang, Q. Fu, B. I. Yakobson, W.-H. Chang, and L.-J. Li, *Nature (London)* **579**, 219 (2020).
- [22] Y. Gao, Z. Liu, D.-M. Sun, L. Huang, L.-P. Ma, L.-C. Yin, T. Ma, Z. Zhang, X.-L. Ma, L.-M. Peng, H.-M. Cheng, and W. Ren, *Nat. Commun.* **6**, 8569 (2015).
- [23] J.-S. Rhyee, J. Kwon, P. Dak, J. H. Kim, S. M. Kim, J. Park, Y. K. Hong, W. G. Song, I. Omkaram, M. A. Alam, and S. Kim, *Adv. Mater.* **28**, 2316 (2016).
- [24] J. Chen, X. Zhao, S. J. R. Tan, H. Xu, B. Wu, B. Liu, D. Fu, W. Fu, D. Geng, Y. Liu, W. Liu, W. Tang, L. Li, W. Zhou, T. C. Sum, and K. P. Loh, *J. Am. Chem. Soc.* **139**, 1073 (2017).
- [25] R. T. Wu, I. K. Drozdov, S. Eltinge, P. Zahl, S. Ismail-Beigi, I. Bozovic, and A. Gozar, *Nat. Nanotechnol.* **14**, 44 (2019).
- [26] M. Batmunkh, M. Bat-Erdene, and J. G. Shapter, *Adv. Mater.* **28**, 8586 (2016).
- [27] A. Carvalho, M. Wang, X. Zhu, A. S. Rodin, H. Su, and A. H. Castro Neto, *Nat. Rev. Mater.* **1**, 16061 (2016).
- [28] Z. Zhu and D. Tománek, *Phys. Rev. Lett.* **112**, 176802 (2014).
- [29] J. L. Zhang, S. Zhao, C. Han, Z. Z. Wang, S. Zhong, S. Sun, R. Guo, X. Zhou, C. D. Gu, K. D. Yuan, Z. Y. Li, and W. Chen, *Nano Lett.* **16**, 4903 (2016).
- [30] J. Zeng, P. Cui, and Z. Y. Zhang, *Phys. Rev. Lett.* **118**, 046101 (2017).
- [31] J.-P. Xu, J.-Q. Zhang, H. Tian, H. Xu, W. Ho, and M. Xie, *Phys. Rev. Materials* **1**, 061002(R) (2017).
- [32] J. Gao, G. Zhang, and Y.-W. Zhang, *J. Am. Chem. Soc.* **138**, 4763 (2016).
- [33] L. Qiu, J. C. Dong, and F. Ding, *Nanoscale* **10**, 2255 (2018).
- [34] Z. B. Yang, J. H. Hao, S. G. Yuan, S. H. Lin, H. M. Yau, J. Y. Dai, and S. P. Lau, *Adv. Mater.* **27**, 3748 (2015).
- [35] H. Xu, X. Han, Z. Li, W. Liu, X. Li, J. Wu, Z. Guo, and H. Liu, *Adv. Mater. Interfaces* **5**, 1801048 (2018).
- [36] Y. Xu, X. Shi, Y. Zhang, H. Zhang, Q. Zhang, Z. Huang, X. Xu, J. Guo, H. Zhang, and L. Sun, *Nat. Commun.* **11**, 1330 (2020).
- [37] Z. Wu, Y. Lyu, Y. Zhang, R. Ding, B. Zheng, Z. Yang, S. P. Lau, X. H. Chen, and J. Hao, *Nat. Mater.* **20**, 1203 (2021).
- [38] F. Xia, H. Wang, J. C. M. Hwang, A. H. Castro Neto, and L. Yang, *Nat. Rev. Phys.* **1**, 306 (2019).
- [39] I. Pletikosić, F. vonRohr, P. Pervan, P. K. Das, I. Vobornik, R. J. Cava, and T. Valla, *Phys. Rev. Lett.* **120**, 156403 (2018).
- [40] Z. Y. Zhang and M. G. Lagally, *Science* **276**, 377 (1997).
- [41] P. Wu, Y. Zhang, P. Cui, Z. Li, J. L. Yang, and Z. Y. Zhang, *Phys. Rev. Lett.* **114**, 216102 (2015).
- [42] P. E. Blöchl, *Phys. Rev. B* **50**, 17953 (1994).
- [43] G. Kresse and J. Furthmüller, *Phys. Rev. B* **54**, 11169 (1996).
- [44] J. P. Perdew, K. Burke, and M. Ernzerhof, *Phys. Rev. Lett.* **77**, 3865 (1996).
- [45] S. Grimme, J. Antony, S. Ehrlich, and H. Krieg, *J. Chem. Phys.* **132**, 154104 (2010).
- [46] J. Heyd, G. E. Scuseria, and M. Ernzerhof, *J. Chem. Phys.* **118**, 8207 (2003).
- [47] G. Henkelman, B. P. Uberuaga, and H. Jónsson, *J. Chem. Phys.* **113**, 9901 (2000).
- [48] S. Nosé, *J. Chem. Phys.* **81**, 511 (1984).
- [49] B. VanTroeye, A. Lherbier, J.-C. Charlier, and X. Gonze, *Phys. Rev. Materials* **2**, 074001 (2018).
- [50] L. Huang and J. Li, *Appl. Phys. Lett.* **108**, 083101 (2016).
- [51] X. Liu, J. D. Wood, K.-S. Chen, E. K. Cho, and M. C. Hersam, *J. Phys. Chem. Lett.* **6**, 773 (2015).
- [52] A. Kundu, D. Tristant, N. Sheremetyeva, A. Yoshimura, A. Torres Dias, K. S. Hazra, V. Meunier, and P. Puech, *Nano Lett.* **20**, 5929 (2020).
- [53] J. C. Jamieson, *Science* **139**, 1291 (1963).
- [54] See Supplemental Material at <http://link.aps.org/supplemental/10.1103/PhysRevB.104.235415> which includes supplemental figures.
- [55] N. Han, N. Gao, and J. Zhao, *J. Phys. Chem. C* **121**, 17893 (2017).
- [56] H. Chen, W. G. Zhu, and Z. Y. Zhang, *Phys. Rev. Lett.* **104**, 186101 (2010).
- [57] X. S. Li, W. W. Cai, L. Colombo, and R. S. Ruoff, *Nano Lett.* **9**, 4268 (2009).
- [58] Y. W. Mo, *Science* **261**, 886 (1993).
- [59] K. Xu, Y. Xu, H. Zhang, B. Peng, H. Shao, G. Ni, J. Li, M. Yao, H. Lu, H. Zhu, and C. M. Soukoulis, *Phys. Chem. Chem. Phys.* **20**, 30351 (2018).
- [60] R. Gillen and J. Maultzsch, *Phys. Rev. B* **97**, 165306 (2018).
- [61] P. Rivera, J. R. Schaibley, A. M. Jones, J. S. Ross, S. Wu, G. Aivazian, P. Klement, K. Seyler, G. Clark, N. J. Ghimire, J. Yan, D. G. Mandrus, W. Yao, and X. D. Xu, *Nat. Commun.* **6**, 6242 (2015).

- [62] M.-H. Chiu, C. Zhang, H.-W. Shiu, C.-P. Chuu, C.-H. Chen, C.-Y. S. Chang, C.-H. Chen, M.-Y. Chou, C.-K. Shih, and L.-J. Li, *Nat. Commun.* **6**, 7666 (2015).
- [63] F. C. Wu, T. Lovorn, and A. H. MacDonald, *Phys. Rev. Lett.* **118**, 147401 (2017).
- [64] S. Latini, K. T. Winther, T. Olsen, and K. S. Thygesen, *Nano Lett.* **17**, 938 (2017).
- [65] D. A. Ruiz-Tijerina and V. I. Fal'ko, *Phys. Rev. B* **99**, 125424 (2019).
- [66] G. Onida, L. Reining, and A. Rubio, *Rev. Mod. Phys.* **74**, 601 (2002).
- [67] D. Y. Qiu, H. Felipe, and S. G. Louie, *Phys. Rev. Lett.* **111**, 216805 (2013).
- [68] J.-H. Choi, P. Cui, H. Lan, and Z. Y. Zhang, *Phys. Rev. Lett.* **115**, 066403 (2015).
- [69] D. Neuhauser, Y. Gao, C. Arntsen, C. Karshenas, E. Rabani, and R. Baer, *Phys. Rev. Lett.* **113**, 076402 (2014).
- [70] W. Hu, L. Lin, R. Q. Zhang, C. Yang, and J. L. Yang, *J. Am. Chem. Soc.* **139**, 15429 (2017).
- [71] F.-C. Wu, F. Xue, and A. H. MacDonald, *Phys. Rev. B* **92**, 165121 (2015).
- [72] Z. Wang, D. A. Rhodes, K. Watanabe, T. Taniguchi, J. C. Hone, J. Shan, and K. F. Mak, *Nature (London)* **574**, 76 (2019).
- [73] R. Fei, W. Kang, and L. Yang, *Phys. Rev. Lett.* **117**, 097601 (2016).
- [74] K. Chang, F. Küster, B. J. Miller, J.-R. Ji, J.-L. Zhang, P. Sessi, S. Barraza-Lopez, and S. S. P. Parkin, *Nano Lett.* **20**, 6590 (2020).
- [75] Z.-Q. Shi, H. Li, Q.-Q. Yuan, C.-L. Xue, Y.-J. Xu, Y.-Y. Lv, Z.-Y. Jia, Y. Chen, W. Zhu, and S.-C. Li, *ACS Nano* **14**, 16755 (2020).
- [76] J. Ji, X. Song, J. Liu, Z. Yan, C. Huo, S. Zhang, M. Su, L. Liao, W. Wang, Z. Ni, Y. Hao, and H. Zhang, *Nat. Commun.* **7**, 13352 (2016).
- [77] G. Bian, X. Wang, Y. Liu, T. Miller, and T.-C. Chiang, *Phys. Rev. Lett.* **108**, 176401 (2012).
- [78] M. Fortin-Deschenes, O. Waller, T. O. Menten, A. Locatelli, S. Mukherjee, F. Genuzio, P. L. Levesque, A. Hebert, R. Martel, and O. Moutanabbir, *Nano Lett.* **17**, 4970 (2017).
- [79] X. Wu, Y. Shao, H. Liu, Z. Feng, Y.-L. Wang, J.-T. Sun, C. Liu, J.-O. Wang, Z.-L. Liu, S.-Y. Zhu, Y.-Q. Wang, S.-X. Du, Y.-G. Shi, K. Ibrahim, and H.-J. Gao, *Adv. Mater.* **29**, 1605407 (2017).
- [80] Y. Shao, Z.-L. Liu, C. Cheng, X. Wu, H. Liu, C. Liu, J.-O. Wang, S.-Y. Zhu, Y.-Q. Wang, D.-X. Shi, K. Ibrahim, J.-T. Sun, Y.-L. Wang, and H.-J. Gao, *Nano Lett.* **18**, 2133 (2018).
- [81] Y. H. Song *et al.* (private communication).